The Boltzmann constant from the H2 18O vibration–rotation spectrum: complementary tests and revised uncertainty budget

The Boltzmann constant from the $H_2{}^{18}O$ vibration-rotation spectrum: Complementary tests and revised uncertainty budget

Eugenio Fasci,[1] Maria Domenica De Vizia,[1] Andrea Merlone,[2] Luigi Moretti,[1] Antonio Castrillo,[1] and Livio Gianfrani[1,*]

[1]*Dipartimento di Matematica e Fisica, Seconda Università di Napoli, Viale Lincoln 5, 81100 Caserta, Italy*
[2]*INRIM, Istituto Nazionale di Ricerca Metrologica, Torino, Italy*
** livio.gianfrani@unina2.it*

Abstract

We report on complementary tests and measurements regarding our recent determination of the Boltzmann constant, k_B, by means of Doppler broadening thermometry, also providing additional information, as compared to previous articles. A revised uncertainty budget is illustrated, including some new components that were ignored in previous spectroscopic experiments, and better quantifying other components that were estimated to be negligible. In particular, we consider the relativistic Doppler effect, the perturbation caused by the finite bandwidth of the detection system as well as the influence of the spontaneous emission content of the probe laser. The new entries do not increase the global uncertainty that still amounts to 24 ppm. Our value for the Boltzmann constant results to be 1.380631 (33) 10^{-23} J/K, which is still the best determination reported so far by using an optical method.

1. INTRODUCTION

Discovered by the Austrian physicist Christian Andreas Doppler in 1841, while looking at the colour of binary stars, the Doppler effect can be regarded as a gift of nature, allowing one to get information about the temperature of any gaseous system, including stellar and planetary atmospheres, interstellar gas clouds, exhaust gases from combustion processes, plasma plumes from laser ablation or flames. It has been known for decades that the temperature of a gaseous mixture could be inferred from the line shape corresponding to a single component of the absorption spectrum of one of its constituents. Examples in the literature can be found even before the advent of tunable lasers. For instance, measurements of upper atmospheric temperatures were routinely performed in the 1960's by means of interferometric spectroscopy, when applied to the determination of the Doppler width of a given, well-isolated, atomic oxygen line in auroras [1].

Very recently, the expression of the Doppler width of a spectral line, valid for a gaseous sample at the thermodynamic equilibrium, has attracted the interest of the international community of fundamental metrology, as it represents a powerful tool to link the thermodynamic temperature to an optical frequency, passing through the Avogadro number and the Boltzmann constant [2]. This is the basis of a relatively new method of primary gas thermometry, known as Doppler broadening thermometry (DBT), which is currently at the stage of further development and optimization.

DBT consists in retrieving the Doppler width ($\Delta\nu_D$) from the highly accurate observation of the spectral profile corresponding to a given atomic or molecular line in a gas sample at the thermodynamic equilibrium [3]. If implemented at the temperature of the triple point of water (namely, T = 273.16 K), pursuing the highest levels of precision and accuracy for laser absorption spectroscopy in the linear regime of interaction, DBT can provide an optical determination of the Boltzmann constant (k_B), by inverting the following equation:

$$\Delta\nu_D = \frac{\nu_0}{c}\sqrt{2\ln 2\frac{k_B T}{M}}\,, \tag{1}$$

being ν_0 the line center frequency, c the speed of light, and M the molecular mass.

In proof-of-principle experiments, performed on NH_3 and CO_2 molecules, k_B was determined with a combined uncertainty of 190 and 160 parts in 10^6, respectively [4,5]. The ammonia infrared spectrum was probed by a frequency-stabilized CO_2 laser, while an extended-cavity diode laser (ECDL) at 2 μm was used to interrogate a vibration–rotation transition of carbon dioxide. In these first experiments, the spectral analysis was performed by using either Gaussian or modified Voigt profiles. In the last few years, with the ambitious goal of approaching the target accuracy of one part in 10^6, technical improvements of the experimental setups are being accompanied by more and more refined modeling of the line shapes. Also, other molecular targets are being considered as thermometric substance, such as water, oxygen and acetylene [6-9]. In any case, an indispensible prerequisite for low-uncertainty DBT is the choice of a well isolated line. In fact, the presence of interfering lines, even when they have a line intensity factor significantly smaller than that of the selected line (namely, 2 or 3 orders of magnitude weaker), can lead to measurable systematical deviations, unless they are properly accounted for in the line fitting procedure. From this point of view, a low-pressure atomic vapor system, like Rb or Cs, should be preferred because of the simplified structure of its absorption spectrum. Furthermore, since the vapor pressure can be very small (down to 10^{-5} Pa), collisions are extremely rare so that pressure-induced variation of the line shape can be completely neglected [10]. On the other hand, the spectra of alkali (or alkali-earth) metal atoms present other difficulties, such as the strong sensitivity to magnetic fields, the relatively large hyperfine structure and the occurrence of optical pumping effects, which should be carefully accounted for, as demonstrated elsewhere [10]. Furthermore, the operation at the temperature of the triple point of water is not straightforward because of the extremely small vapor pressure ($3\ 10^{-6}$ Pa for Rb, $9\ 10^{-8}$ Pa for K, 10^{-20} Pa for Sr, just to mention a few examples).

Going back to molecular samples, carbon dioxide surely offers several advantages: it is a linear molecule without a permanent electric dipole moment, it shows no hyperfine structure, and it is practically insensitive to magnetic fields, like many other diamagnetic molecules. The only drawback is related to the line intensity factors, which are rather small in the near-infrared (NIR) portion of the electromagnetic spectrum. In the wavelength window around 2 μm, vibration-rotation transitions exhibit a linestrength between 10^{-22} and 10^{-21} cm/molecule, while at 1.5 μm the typical intensity amounts to 10^{-23} cm/mol. From this point of view, water is much more advantageous because of the relatively small mass, which leads to large vibrational frequencies. As a matter of fact, the spectral lines of the $2\nu_1$ and $\nu_1+\nu_3$ bands, occurring at 1.4 μm, can have an intensity as large as 10^{-20} cm/mol. Being a light molecule, it also shows a larger Doppler width, as compared to CO_2 and other heavier molecules with absorption features in the NIR. Furthermore, the hyperfine structure can be neglected, as magnetic dipole and electric quadrupole effects do not occur. More particularly, hyperfine splitting should be produced for transitions of the *ortho* type only by spin–spin and spin–rotation interactions [11]. Nevertheless, these effects are so small that the resulting splitting (of the order of few tens of kHz) is 4-5 orders of magnitude smaller than the Doppler width of the line, while it is totally absent for *para* transitions [12]. These were the reasons that led us to select water in our DBT implementation. In order to reduce the influence of water absorption along the beam-path in air, we selected an isolated line of the ^{18}O-isotopologue.

It is worth noting that the discussion above has been limited to the spectral window between 0.9 and 1.7 μm. This is because in that spectral region InGaAs detectors are available, showing superb

characteristics in terms of noise equivalent power and linearity, much better than mid-infrared detectors [13].

In the present paper, we report complementary tests and information regarding our recent implementation of the DBT methodology, which allowed use to obtain the best optical determination of the Boltzmann constant, reported so far [14]. We will discuss possible sources of systematical deviations that were ignored in previous publications, such as the distortion of the absorption line shape resulting from the finite bandwidth of the detection system, the possible difference between the optical zero and the electrical zero caused by the out-of-resonance radiation transported by the probe laser, and the relativistic Doppler effect. Furthermore, we provide new elements supporting the validity of the choice of the line shape model, including the linear dependence of the collisional width and of the velocity-changing collision frequency on the water vapor pressure.

2. EXPERIMENTAL DETAILS

Figure 1 shows a sketch of the laser absorption spectrometer. It basically consists of an extended cavity diode laser (ECDL), namely, the probe laser, with an emission wavelength in the range between 1.38 and 1.41 μm (provided by TOPTICA, model DL100), a frequency control system, an intensity stabilization feed-back loop, and an isothermal cell. Precise control, stabilization and synchronization of the laser frequency is achieved by using the technique of offset-frequency locking, in which the probe laser is forced to maintain a precise frequency-offset from a reference laser, which is an ECDL too [15]. This offset is provided by a radio-frequency (rf) synthesizer, which in turn is phase-locked to an ultra-stable Rb oscillator. The reference ECDL (SACHER Lynx S3) presents a sub-kilohertz absolute stabilization of its central frequency, being locked to an ultra-narrow saturated absorption signal, resulting from the nonlinear interaction that occurs inside a high-finesse optical resonator, in coincidence with a particular vibration-rotation line of the $H_2{}^{18}O$ isotopologue. More particularly, the ECDL is locked to a high finesse optical cavity by means of the Pound-Drever-Hall technique. Then, the cavity-mode frequency is actively stabilized against the center of the sub-Doppler feature by using an error signal that is provided by the first-derivative detection of the cavity transmission, after dithering the cavity resonance by means of a sinusoidal voltage-signal at 2 kHz. It is worth noting that this dither is transferred from the reference laser to the probe laser, the modulation frequency being well within the bandwidth of the offset-frequency locking loop. As a consequence, a broadening of the emission width of the probe laser takes place, up to the level of ~1 MHz. This has to be considered in the uncertainty budget for the spectroscopic determination of k_B and, in fact, represents one of the main sources of type-B uncertainty.

The beat note between the two lasers is first detected by means of a fast photodiode (New Focus, model 1567-A), properly amplified (by 20 dB, using the rf amplifier RF Bay LPA-8-17), scaled in frequency (by means of a high-speed frequency-divider, RF Bay, FPS-10-12), and subsequently compared with the rf signal, so as to produce an error signal driving the probe laser. To this purpose, a digital phase and frequency detector, with an integrated loop filter (RF Bay, PDF100, with a bandwidth of 10 kHz), was used. The error signal drives a double-servo system, which acts on the injection current (passing through the current driver) and on the extended-cavity length (by means of a piezoelectric transducer) of the probe ECDL. By tuning the rf frequency, it is possible to perform continuous, highly linear and highly accurate frequency scans of the probe laser around a given center frequency.

The most subtle source of systematic deviations, namely, amplitude variations in the background baseline, are essentially removed by implementing an intensity control feedback loop, based upon

an acousto-optic modulator, which effectively compensates for any power variation associated to a laser frequency scan, as well as for the periodic modulation of the power arising from spurious etalon effects. Intensity stabilization at the level of one part in 10^4 was achieved over a frequency scan as wide as 10 GHz, the bandwidth of the control loop being ~50 kHz.

Spectral filtering of the probe laser beam is performed by using a diffraction grating (with 1200 lines/mm) in conjunction to an iris diaphragm (whose aperture has a diameter of 2 mm), the distance between the two being 2.5 m. This scheme allowed us to reduce the spontaneous emission content on the probe laser from ~2% down to ~1.5 10^{-6}.

Equipped with a pair of antireflection-coated BK7 windows, the isothermal cell is 150-mm long and it is referenced to the triple point of water (TPW), with temperature accuracy, uniformity and stability at the level of 0.1 mK, as extensively described elsewhere [16].

Finally, the transmitted beam is detected by means of a ultralow-noise, preamplified, InGaAs photodiode (see the beam path drawn in figure 1), whose electrical bandwidth is set to 1 kHz. The preamplifier consists of a transimpedance amplifier, which also acts as a first-order active low-pass filter.

High quality optical components were used, with an anti-reflection coating at 1.4 μm showing a residual reflectivity equal to (or smaller than) 0.1%; the surface irregularity was λ/10, while a 10:5 scratch-dig characterizes the surface quality of lenses, beam splitters and optical windows (provided by CVI Laser Optics).

Absorption spectra are acquired using a data acquisition board (ADC) with a 16-bit resolution and a sampling rate of 10^6 samples per second. The possible nonlinearity of the whole detection chain was estimated to be well below the noise level. A LABVIEW code allows us to control the whole setup, to perform step-by-step frequency scans and to acquire, for each step, the transmitted signal.

3. RESULTS AND DISCUSSION

The isothermal cell was filled with a 97.7% enriched ^{18}O water sample at variable pressures. The total number of acquired spectra was 718, in coincidence with the $4_{4,1} \rightarrow 4_{4,0}$ transition of the $H_2{}^{18}O$ $\nu_1 + \nu_3$ band, recorded at the TPW temperature as a function of the total gas pressure. Figure 2 shows an example spectrum, acquired at a pressure of about 400 Pa. The laser scan was typically 3.1 GHz wide and resulted from 3100 steps of 1 MHz each, with a step-by-step acquisition time of 100 ms. The signal-to-noise ratio was measured to be about 5000, the noise level being a factor of 100 above the shot-noise limit.

3.1 The influence of the detection bandwidth

The finite bandwidth of the detection system can cause distortions to the measured line shape. Very recently, a theoretical model has been developed in order to consider the influence of the detection bandwidth properties on the observed line shapes in laser absorption spectroscopy [17]. The model predicts artificial frequency shifts, extra broadenings and line asymmetries which must be taken into account in order to obtain accurate line parameters. The theoretical model has been validated by experiments performed on H_2O and NH_3 molecular lines recorded by precision laser spectroscopy, in the near- and mid- infrared spectral regions [17]. Furthermore, it has been possible to figure out the detection bandwidth adjustments required to perform a spectroscopic determination of the Boltzmann constant at the 1 ppm level of accuracy (ppm standing for part per million). In this respect, an important parameter is the so-called frequency constant, ν_D, which is given by the

product between the filter time constant, τ_D, and the scan rate, $\dot{\nu} = \Delta\nu / \Delta t$, $\Delta\nu$ being the frequency step and Δt the time interval for each step. For a Voigt profile, assuming a continuous sweep of the laser frequency, it turns out that the Gaussian contribution appears to be different from the Doppler width of the line, according to the formula [17]:

$$\Delta\nu_G = \sqrt{\Delta\nu_D^2 + (2 - 4Q^2)\nu_D^2 \ln 2}\,, \tag{2}$$

Q being the quality factor of the filter and $\Delta\nu_G$ the apparent Doppler width (HWHM). Properly designed experiments have shown that this formula applies also to the case of a step-by-step frequency scan, even when using more sophisticated line shape models for the spectral analysis. In other words, by inverting Eq. (2), it is possible to correct for the systematical deviation in Doppler width retrieval that is caused by the filter, reaching an agreement between the corrected values and the expected ones at the level of $6\text{x}10^{-3}$, for ν_D values ranging between 1 and 500.

For the first-order filter of the present experiment (with -6 dB/octave roll-off and Q=0), being $\dot{\nu}$=10 MHz/s and ν_D=1.59 kHz, the relative shift in the Doppler width amounts to 2 parts over 10^{11}, which translates into a type-B uncertainty on k_B of $4\text{x}10^{-11}$.

3.2 The limited spectral purity of the probe laser

In absorption spectrometry and, more importantly, in Doppler broadening thermometry, another possible source of systematical deviation can be ascribed to the limited spectral purity of the probe laser. If a small amount of the power is distributed out from the main mode of the laser emission, then the optical zero is not coincident with the zero detected signal (obviously, it is assumed that the signal itself is properly corrected for the detector's electric offset). Specifically, if the main mode of the laser emission is resonant with a given spectral line, the optical zero is defined as the asymptotic value to which the transmitted power tends when increasing the pressure of the absorbing gas, thus approaching a fractional absorption of 100% for the main mode of the probe laser. The spontaneous emission content on the probe laser gives rise to a measurable offset between optical and electrical zero. Therefore, in order to avoid systematical deviations in retrieving spectroscopic quantities (including the Doppler width) from a least-squares fit of an absorption spectrum, it is important to check whether the optical zero is coincident with the electrical zero. It is worth to remind that the absorption process occurring in the sample cell is ruled by the well known Beer-Lambert law, which states that the transmitted power P_t decreases as

$$P_t = P_0 \exp[-S(T)NLg(\tilde{\nu} - \tilde{\nu}_0)]\,, \tag{3}$$

where P_0 is the incident power, $\tilde{\nu}$ the laser wavenumber (given by ν/c and expressed in cm^{-1}) $\tilde{\nu}_0$ the line center wavenumber, L the absorption path length (in cm), N the gas density (in molecules/cm^3), $S(T)$ the transition strength (in cm/molecule) at the gas temperature T, and $g(\tilde{\nu} - \tilde{\nu}_0)$ the line shape function (in cm), this latter being normalized such that $\int g(\tilde{\nu} - \tilde{\nu}_0)d\tilde{\nu} = 1$. Therefore, the fractional absorption at the line center is given by:

$$\frac{\Delta P(\tilde{\nu}_0)}{P_0} = 1 - \exp[-S(T)NLg(0)]\,. \tag{4}$$

Under the assumption of an optical zero coincident with the electrical zero, it follows that the measured fractional absorption should asymptotically tend to 1; alternatively, the convergence

occurs towards a limit (A_0) smaller than 1 by a quantity representing the optical zero, this latter being given by $(1- A_0)P_0$.

In figure 3, we report the measurement of the fractional absorption at the line center, as recorded for the $H_2{}^{18}O$ line of interest after a double pass in a 1-m long gas cell, at the room temperature. The gas pressure was varied between 50 and 1300 Pa; for each of the eighteen pressure values, two spectral acquisitions were performed. For each spectrum, the fractional absorption resulted from the application of a nonlinear least-squares fitting procedure, adopting the speed-dependent Voigt (SDV) profile as a line shape model [18]. The asymptotic convergence towards 1 is clearly visible from the inset of figure 3, with the two points at the highest pressure differing from 1 of about 10^{-6}. This is consistent with what expected on the basis of the spontaneous emission content of the probe laser, after spectral filtering. Such a difference is well within the noise level characterizing our experimental spectra (of the order of 0.4 mV). Unfortunately, a precise evaluation of the asymptotic value was not possible. In fact, a fit of the data of figure 3 was performed using the following equation:

$$\frac{\Delta P(\tilde{\nu}_0)}{P_0} = A_0 - exp[-A_1 p] , \tag{5}$$

where A_1 is equal to $\frac{S(T)Lg(0)}{k_B T}$. The quantities A_0 and A_1 were treated as free parameters. The resulting value of A_0 was 1.0000 ± 0.0009. In other words, the relatively large uncertainty did not allow us to quantify the difference from 1 and, consequently, the optical zero.

Assuming that the optical zero is reached at the highest pressure (leading to a transmitted power of 1.3 $10^{-6}P_0$), it is possible to quantify its influence on the retrieved Doppler widths. Numerical simulations, which were done by means of the Voigt model, allowed us to calculate the associated systematical shift in Doppler-width retrievals, which was positive and dependent on the fractional absorption (and, hence, on the gas pressure). For a line-center absorption of 50%, it amounts to about 0.1 ppm.

3.3 Testing the validity of the choice of the line shape model

A major effort in our work was devoted to line shape modeling, which is far from being trivial for self-colliding water molecules. In fact, deviations from the Voigt model are clearly observed even in the case of pure H_2O samples at relatively small pressures [18]. In this respect, the molecular confinement alone was revealed to be unable to explain entirely these departures, while the speed dependence of pressure-induced broadening and shifting should be taken into account.

Therefore, speed-dependent and Dicke narrowing effects were jointly considered by adopting the so-called partially correlated speed-dependent hard-collision (pcSDHC) model in the nonlinear least-squares fits of the recorded spectra [19]. Recent theoretical and experimental studies have demonstrated that this model is the most appropriate one to describe the physical situation of self-colliding water molecules, even in the Doppler regime [19, 20].

Hence, experimental profiles were fitted to the function here below:

$$P(\nu) = (P_1 + P_2 \cdot \nu) exp[-A \cdot h(\nu - \nu_0)] , \tag{6}$$

where A represents the integrated absorbance, namely $A = S(T)NL$, the parameters P_1 and P_2 account for a residual, linear variation of the incident power, and $h(\nu - \nu_0)$ is the line shape function, as provided by the pcSDHC model. The non-linear, least-squares, fitting procedure was implemented under the MATLAB environment, using the trust region optimization algorithm, and

involved a single spectrum at a time. A total of seven quantities were considered as free parameters, including A, P_1, P_2, the Doppler width, the collision frequency, the collisional shift and width, this latter being averaged over the absorbers' speed. Fit residuals associated to the spectrum of figure 2 are shown in figure 4. The noise level is smaller around the line center, as the transmitted signal is significantly reduced at those frequencies (see figure 2). The pcSDHC model allowed us to successfully fit the measured profiles within the experimental noise, with a root-mean-square (rms) value of the residuals of 0.381 mV. One might be interested in understanding which performance would have been obtained by adopting a simplified model, such as the symmetric version of the speed-dependent Voigt profile. This model allows one to consider line narrowing due to the speed dependence of collisional broadening, ignoring the averaging effect of velocity changing collisions as well as the speed dependence of pressure shift. Looking at the residuals of the lower trace of figure 4, a small w-shaped structure is visible around the line center. This is a clear consequence of the fact that line narrowing effects are not properly accounted for, when using a simplified line shape model. It is also true that the difference between the rms values of the residuals amounts to only 15 μV. Nevertheless, this would be sufficient to add a measurable systematical deviation in Doppler width retrievals (of the order of one part in 10^3).

Figure 5 shows the retrieved Doppler and pressure widths, by applying the pcSDHC model to the analysis of the recorded spectra. It is worth noting that a linear fit of the Doppler width data, as a function of the integrated absorbance, gives a slope perfectly consistent with zero (namely, $-0.06\ 10^{-5} \pm 8\ 10^{-5}$). This is a first important element supporting the validity of the spectral analysis. In fact, the Doppler width, being pressure independent, should not depend on the integrated absorbance. Another strong element is reported in the upper graph of figure 5, in which the retrieved pressure widths are plotted as a function of the total water vapor pressure. Due to technical difficulties in doing reliable measurements of the gas pressure, this latter was determined from the integrated absorbance, by using the HITRAN value for the transition strength, properly rescaled to consider the difference between the actual temperature and the reference temperature adopted in the HITRAN database (that is 296 K) [21]. We also corrected for the different abundances (97.7% in our experiment compared to the atmospheric abundance of $H_2{}^{18}O$, which is 0.1999 %, used in HITRAN). As expected, a linear dependence of the pressure widths on the water vapor pressure is obtained, the linear fit showing a Pearson's correlation coefficient of 0.99398. A similar behavior was found for the retrieved velocity-changing collision frequencies, the Pearson's correlation coefficient being 0.95712, in this case. The linear fit reported in the upper plot of figure 5 gives the pressure broadening coefficient, which resulted to be 13.86 (6) MHz/Torr, in good agreement with the value taken from the HITRAN database, namely 14.0 (7) MHz/Torr at the temperature of the triple point of water.

From the Doppler width data of figure 5, the Boltzmann constant could be retrieved with a relative statistical uncertainty of ~16 ppm. Repeating the complete analysis by using the SDV model, we obtain a different value for k_B, which results to be underestimated by about seven parts over 10^4. Therefore, it is confirmed that the choice of the line shape model is of the utmost importance for a successful low-uncertainty DBT experiment, circumstance that was already hypothesized in previous articles [3, 6].

3.4 The relativistic Doppler effect

Given the unprecedented quality and fidelity in the observation of the absorption spectra, one may wonder whether the relativistic Doppler effect should be considered. At the TPW temperature, the most probable speed of the absorbing molecules (v_m) amounts to about 500 m/s, which gives a β-value (namely, the ratio v_m/c) of about $1.6\ 10^{-6}$. In a recent paper, a relativistic formulation for the

Voigt profile has been provided [24]. A comparison with the classical Voigt profile has revealed that the relativistic deformation, expressed in terms of peak-to-peak relative variation between relativistic and classical Voigt profile, is of the order of few parts over 10^7, for $\beta=10^{-6}$ [24]. This is more than three order of magnitude below the noise level affecting our spectra. Even though a relativistic version of the pcSDHC model is not yet available, a similar deformation is likely to be observed also for this model. Therefore, we can conclude that relativistic effects should be completely negligible.

3.5 The revised uncertainty budget

The complete uncertainty budget is shown in Table 1. Compared to the previous version, reported in Ref. [23], we added the three new components that have been discussed in this Section. Moreover, we quantified the influence of the detector nonlinearity, optical saturation as well as spurious etalon effects.

As for the detector nonlinearity, InGaAs photodiodes show linearity in the response within 0.08% in the photocurrent range from 10^{-7} to 10^{-4} μA [13]. In our experiment, the typical variation of the photocurrent occurs in the interval 20-50 μA, which translates into a nonlinearity within 2 parts in 10^6. We adopted the following procedure to quantify its influence on Doppler width retrieval: we started from a real spectrum, characterized by a fractional absorption of ~60%. The nonlinearity in the vertical scale was added in the form of a second-order polynomial. Subsequently, a nonlinear least-squares fit was repeated for both the original and distorted spectrum, so as to compare the retrieved Doppler widths. We found a relative variation of 0.2 ppm, which increases up to ~1 ppm for a fractional absorption of ~80%. This leads to a type B uncertainty in the determination of k_B of 2 parts over 10^6, which has to be considered as an upper limit to this kind of uncertainty.

As far as optical saturation is concerned, the saturation intensity of the selected line, I_{sat}, for a $H_2{}^{18}O$ pressure of 100 Pa, amounts to 1.1 10^8 W/m^2. This is roughly seven orders of magnitude larger than the intensity of the probe laser, I_0. In the Doppler regime, the absorption coefficient is reduced by a factor $\frac{1}{\sqrt{1+G}}$, G being the degree of saturation that is equal to the ratio I_0/ I_{sat}. The analysis of numerically simulated spectra (also in this case, based on the Voigt model) suggests that the influence on the retrieved Doppler width consists in a positive shift of 1 part in 10^9, which has essentially no influence in our uncertainty budget.

Finally, the analysis of possible amplitude modulations arising from spurious etalon effects require a special attention. In assembling the water spectrometer, a particular care was taken to avoid as much as possible this kind of effect, which is rather common in laser absorption spectroscopy. In this respect, the high quality of all the optical components that were employed was surely crucial in order to limit as much as possible the occurrence of etalon effects. As a result, it is rather difficult to recognize possible interference fringes from either acquire spectra or fits' residuals. Nevertheless, to further investigate this issue, it is possible to make use of signal processing tools like the Savitzky–Golay filter, based upon successive fitting of sub-sets of adjacent points by means of a low-degree polynomial function. The application of such a smoothing method to the residuals of the upper graph of figure 4 resulted in the plot of figure 6. The situation is surely improved in terms of signal-to-noise ratio, so that it becomes possible to catch a periodic modulation that could be ascribed to an etalon effect. The coherent structure in the residuals suggests a free-spectral range of ~70 MHz and a peak-to-peak amplitude smaller than 0.4 mV. Also in this case, the analysis of numerically simulated spectra, to which this kind of coherent noise is

superimposed, gives quantitative information on the type B error that might be caused by the etalon effect. Its turns out a positive deviation in the retrieved Doppler width of 0.6 ppm.

It is worth noting that the new entries in Table 1 do not increase the global uncertainty that still amounts to 24 ppm. Therefore, our value for the Boltzmann constant results to be unchanged, namely, 1.380631 (33) 10^{-23} J/K [14], in full agreement with the recommended CODATA value [25].

4. CONCLUSIONS

Complementary tests, measurements and analysis, related to our recent determination of the Boltzmann constant, have been reported. The uncertainty budget has been revised, quantifying those components that were estimated to be negligible in previous articles. Furthermore, the budget has been completed by adding three new components whose effect, however, is well below the ppm level. On the hand, it is confirmed the great potential of Doppler broadening thermometry, on the other hand it is clear that several factors must be carefully considered to further decrease the global uncertainty and make DBT really competitive with more consolidated techniques, like acoustic gas thermometry [26] or dielectric constant gas thermometry [27].

We are presently working on a 3rd-generation spectrometer that should allow us to significantly reduce the three main sources of uncertainty. First of all, the limitation arising from FM broadening has been completely removed, by implementing the technique known as noise-immune cavity-enhanced optical heterodyne molecular spectroscopy (NICE-OHMS) for the highly-sensitive detection of the sub-Doppler $H_2{}^{18}O$ line, on which the reference laser is stabilized [28]. In this respect, we exploit the fact that NICE-OHMS provides a dispersion signal without dithering the optical cavity, likely to be employed as an error signal. Similarly, the spectral purity of the probe laser has been improved by means of optical phase-locking to the reference laser.

In the new spectrometer, the isothermal cell consists in a spherical, Herriott-type, multiple reflection cell with a maximum path-length of ~12 m in a volume of ~4 10^{-4} m^3. This important upgrade will allow us to significantly reduce the gas pressure (down to 1 Pa) and, possibly, simplify the spectral analysis so as to reduce the uncertainty associated to the line shape model. To this purpose, but also to reduce the statistical uncertainty, a global fitting code has been developed in the MATLAB environment using a variety of semiclassical line shape models. It allows one to simultaneously fit a manifold of spectra across a given range of pressures, sharing a restricted number of unknown parameters, including the Doppler width. This feature, along with physical constraints that can be easily implemented in a global fitting approach, is expected to reduce the statistical correlation among the free parameters. The complete description and test of the new spectral analysis procedure will be the subject of another article.

It is worth noting that absorption spectra, when acquired with the highest metrological qualities, can provide information on other physical quantities, besides the Doppler width. For instance, we have shown that the integrated absorbance is proportional to the molecular number density, circumstance that has allowed us to perform a spectroscopic determination of the water vapor pressure. Similarly, the same set-up can be employed for highly accurate determinations of the amount of substance. Furthermore, it is possible to perform isotope ratio measurements for the stable isotopologues of water (namely, $^{17}O/^{16}O$, $^{18}O/^{16}O$ and D/H in water) [29]. This latter application requires a proper selection of the wavelength of the probe laser, so as it is possible to catch a pair of vibration-rotation transitions for the isotopologues of interest, within a single scan of the laser itself [30].

ACKNOWLEDGEMENTS

This work was partially performed within the EURAMET project no. 885, entitled "New determinations of the Boltzmann constant", coordinated by Joachim Fischer, PTB-Berlin. We gratefully acknowledge funding from EMRP through Project No. SIB01-REG3 and SIB01-REG4. The EMRP is jointly funded by the EMRP participating countries within EURAMET and the European Union.

REFERENCES

[1] Nilson J A and Shepherd G G 1961 Upper atmospheric temperatures from Doppler line widths – I. Some preliminary observations on OI 5577 Å in aurora. Planetary Space Sci. **5** 299-306.

[2] Bordé C J 2002 Atomic clocks and inertial sensors. Metrologia **39** 435–463.

[3] Gianfrani L 2012 Highly-accurate line shape studies in the near-IR spectrum of $H_2{}^{18}O$: Implications for the spectroscopic determination of the Boltzmann constant. J. Phys.: Conf. Ser. **397** 012029 1-7.

[4] Daussy C, Guinet M, Amy-Klein A, Djerroud K, Hermier Y, Briaudeau S, Bordé C J, Chardonnet C 2007 Direct determination of the Boltzmann constant by an optical method. Phys. Rev. Lett. **98** 250801.

[5] Casa G, Castrillo A, Galzerano G, Wehr R, Merlone A, di Serafino D, Laporta P, Gianfrani L 2008 Primary gas thermometry by means of laser-absorption spectroscopy: Determination of the Boltzmann constant. Phys. Rev. Lett. **100** 200801.

[6] De Vizia M D, Moretti L, Castrillo A, Fasci E, and Gianfrani L 2011 The line shape problem in Doppler-width thermometry. Mol. Physics **39** 2291-2298.

[7] Cygan A, Lisak D, Trawiński R S, Ciurylo R 2010 Influence of line shape model on the spectroscopic determination of the Boltzmann constant. Phys. Rev. A **82** 032515.

[8] Y. R. Sun Y R, Pan H, Cheng C-F, Liu A-W, Zhang J-T, Hu S-M 2011 Application of cavity ring-down spectroscopy to the Boltzmann constant determination. Opt. Express **19** 19993-20002.

[9] Hashemi R, Povey C, Derksen M, Naseri H, Garber J, and Predoi-Cross A 2014 Doppler broadening thermometry of acetylene and accurate measurement of the Boltzmann constant. J. Chem. Phys. **141** 214201 1-7.

[10] Truong G-W, May E F, Stace T M, and Luiten A N 2011 Quantitative atomic spectroscopy for primary thermometry. Phys. Rev. A **83**, 033805 1-9.

[11] Puzzarini C, Cazzoli G, Harding M E, Vázquez J, Gauss J 2009 A new experimental absolute nuclear magnetic shielding scale for oxygen based on the rotational hyperfine structure of $H_2{}^{17}O$. J. Chem. Phys. **131** 234304 1-11.

[12] Cazzoli G, Puzzarini C, Harding M E, Gauss J 2009 The hyperfine structure in the rotational spectrum of water: Lamb-dip technique and quantum-chemical calculations. J. Chem. Phys. Lett. **473** 21-25.

[13] Yoon H W, Butler J J, Larason T C, and Eppeldauer G P 2003 Linearity of InGaAs photodiodes. Metrologia **40** S154–S158.

[14] Moretti L, Castrillo A, Fasci E, De Vizia M D, Casa G, Galzerano G, Merlone A, Laporta P, and Gianfrani L 2013 Determination of the Boltzmann constant by means of precision measurements of $H_2{}^{18}O$ line shapes at 1.39 μm. Phys. Rev. Lett. **111** 060803 1-5.

[15] Castrillo A, Fasci E, Galzerano G, Casa G, Laporta P, and Gianfrani L 2010 Offset-frequency locking of extended-cavity diode lasers for precision spectroscopy of water at 1.38 μm. Opt. Express **18** 21851–21860.

[16] Merlone A, Moro F, Castrillo A, and Gianfrani L 2010 Design and Capabilities of the Temperature Control System for the Italian Experiment Based on Precision Laser Spectroscopy for a New Determination of the Boltzmann Constant. Int. J. Thermophys. **31** 1360-1370.
[17] Rohart F, Mejri S, Sow P L T, Tokunaga S K, Chardonnet C, Darquié B, Dinesan H, Fasci E, Castrillo A, Gianfrani L, and Daussy C 2014 Absorption line shape recovery beyond the detection bandwidth limit: application to the Boltzmann constant determination. Phys. Rev. A **90** 042506 1-12.
[18] De Vizia M D, Rohart F, Castrillo A, Fasci E, Moretti L, Gianfrani L 2011 Speed-dependent effects in the near-infrared spesctrum of self-colliding $H_2{}^{18}O$ molecules. Phys. Rev. A **83** 052506 1-8.
[19] Ngo N H, Tran H, and Gamache R R 2012 A pure H_2O isolated line-shape model based on classical molecular dynamics simulations of velocity changes and semi-classical calculations of speed-dependent collisional parameters. J. Chem. Phys. **136** 154310 1-8.
[20] Tran H, Ngo N H, Hartmann J-M, Gamache R R, Mondelain D, Kassi S, Campargue A, Gianfrani L, Castrillo A, Fasci E, and Rohart F 2013 Velocity effects on the shape of pure H_2O isolated lines: Complementary tests of the partially correlated speed-dependent Keilson-Storer model. J. Chem. Phys. **138** 034302 1-8.
[21] Rothmann L S et al 2013 The HITRAN2012 molecular spectroscopic database. J. Quantum Spectrosc. Radiat. Transfer **130** 4-50.
[22] Lemarchand C, Triki M, Darquié B, Bordé C J, Chardonnet C, and Daussy C 2011 Progress towards an accurate determination of the Boltzmann constant by Doppler spectroscopy. New J. Phys. **13** 073028 1-22.
[23] Castrillo A, Moretti L, Fasci E, De Vizia M D, Casa G, and Gianfrani L 2014 The Boltzmann constant from the shape of a molecular spectral line. J. Mol. Spectr. **300** 131–138.
[24] Wcislo P, Amodio P, Ciurylo R, and Gianfrani L 2014 Relativistic formulation of the Voigt profile. Phys. Rev. A, in press.
[25] Mohr P J, Taylor B N, and Newell D B 2012 CODATA Recommended Values of the Fundamental Physical Constants: 2010. Rev. Mod. Phys. **84** 1527-1605.
[26] Moldover M R, Gavioso R M, Mehl J B, Pitre L, de Podesta M and Zhang J T 2014 Acoustic Gas Thermometry. Metrologia **51** R1-R19.
[27] Fellmuth B, Fischer J, Gaiser C, Jusko O, Priruenrom T, Sabuga W, Zandt T (2013) Improved determination of the Boltzmann constant by dielectric-constant gas thermometry. Metrologia **50** L7–L11.
[28] Dinesan H, Fasci E, Castrillo A, and Gianfrani L 2014 Absolute frequency stabilization of an extended-cavity diode laser by means of noise-immune cavity-enhanced optical heterodyne molecular spectroscopy. Opt. Lett. **39** 2198–2201.
[29] Castrillo A, Dinesan H, Casa G, Galzerano G, Laporta P, and Gianfrani L 2012 Amount-ratio determinations of water isotopologues by dual-laser absorption spectrometry. Phys. Rev. A, **86** 052515 1-7.
[30] Kerstel E and Gianfrani L 2008 Advances in laser-based isotope ratio measurements: Selected applications. Appl. Phys. B **92** 439-449.

Table 1. Uncertainty budget (in terms of relative contributions, corresponding to one standard deviation) related to the spectroscopic determination of the Boltzmann constant.

Components from Ref. [23]	**Type A**	**Type B**
Reproducibility of Doppler width measurements	15.7×10^{-6}	
Frequency scale		$< 2 \times 10^{-6}$
Line-center frequency		0.278×10^{-6}
Line emission width and FM broadening		10×10^{-6}
Optical saturation effects		10^{-9}
Detector nonlinearity		$< 2\ 10^{-6}$
AM modulation effects		$< 1.2\ 10^{-6}$
Cell's temperature	3.7×10^{-8}	1.1×10^{-6}
Hyperfine structure effects		$< 10^{-6}$
Line shape model		14.9×10^{-6}
New components		
Finite detection bandwidth		4×10^{-11}
Relativistic effects		negligible
Optical zero		$< 2 \times 10^{-7}$
Combined relative uncertainty = 24×10^{-6}		

Figure 1. Sketch of the laser absorption spectrometer developed at the wavelength of 1.39 μm. M stands for mirror, L for lens, SM for spherical mirror, BS for beam-splitter, Ph for photodiode, FPh for fast photodetector, G for diffraction grating, AOM for acousto-optic modulator, ADC for analog-to-digital converter.

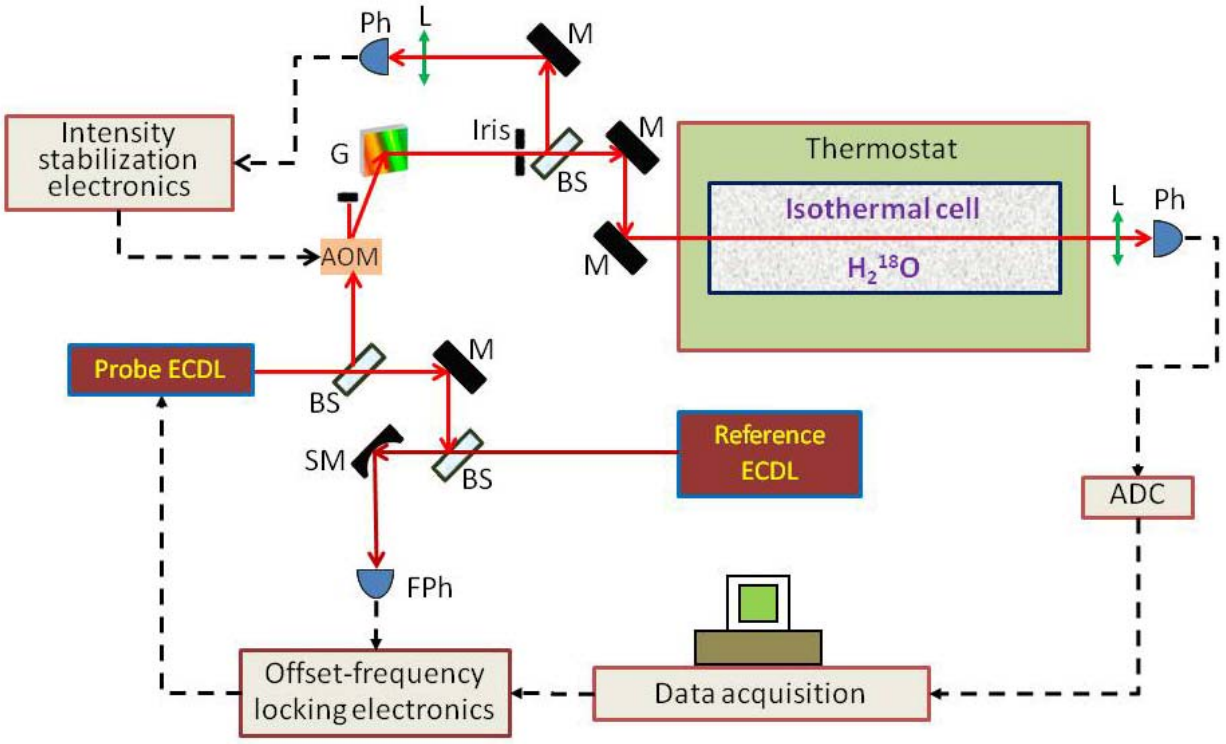

Figure 2. Example of an absorption spectrum. The x-axis represents the frequency detuning from the center of the $4_{4,0} \rightarrow 4_{4,1}$ line of the $H_2{}^{18}O$ $\nu_1 + \nu_3$ band that is used for the absolute stabilization of the reference laser.

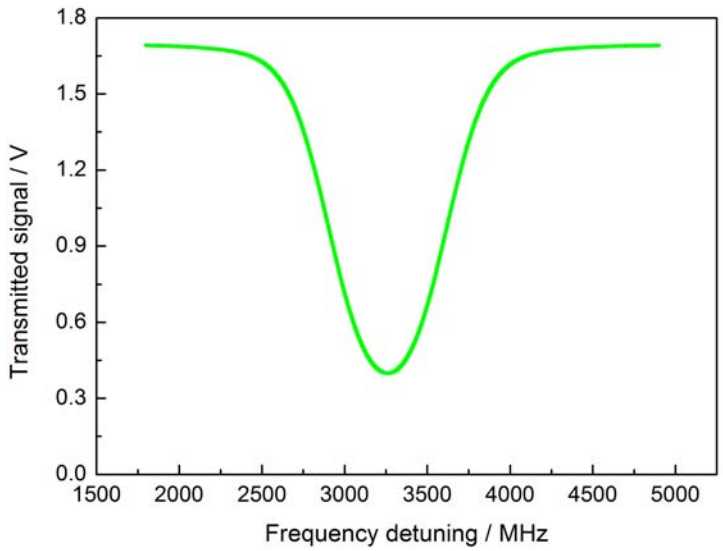

Figure 3. Determination of the optical zero.

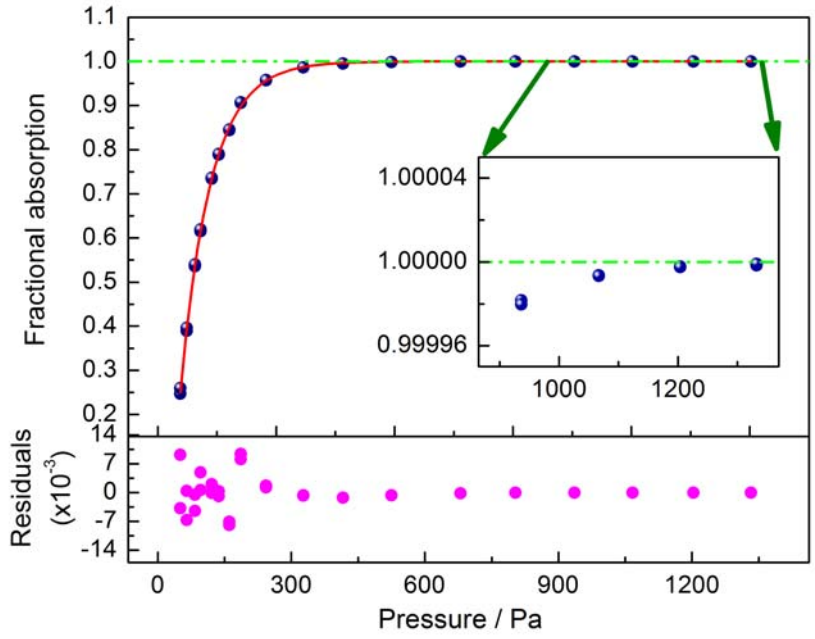

Figure 4. Fit residuals by using the pcSDHC model (upper plot) and the speed-dependent Voigt (SDV) profile (lower trace). Root-mean square values are also reported.

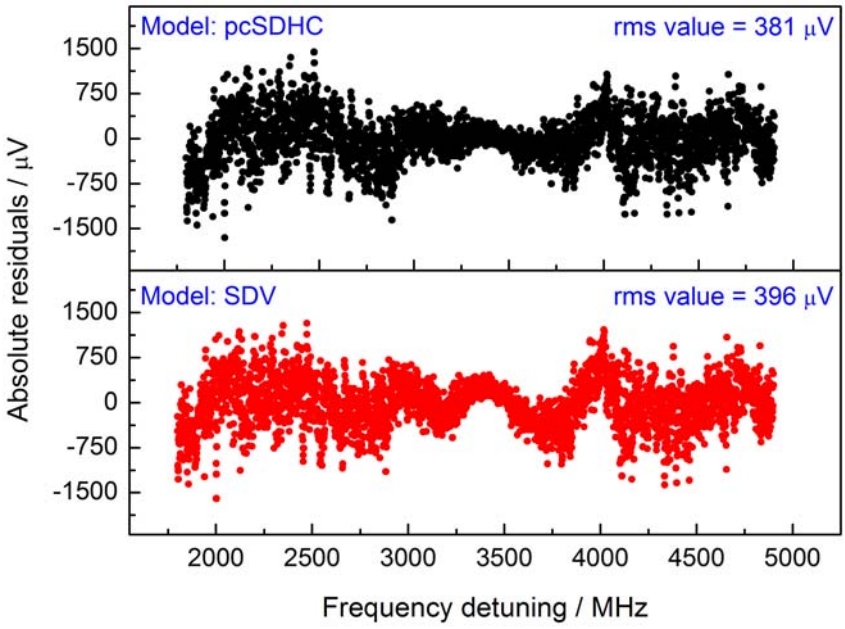

Figure 5. Doppler widths and pressure widths as retrieved from the nonlinear least-squares fits of the recorded spectra. The former are plotted as a function of the integrated absorbance (lower panel), while the latter are reported as a function of the water vapor pressure.

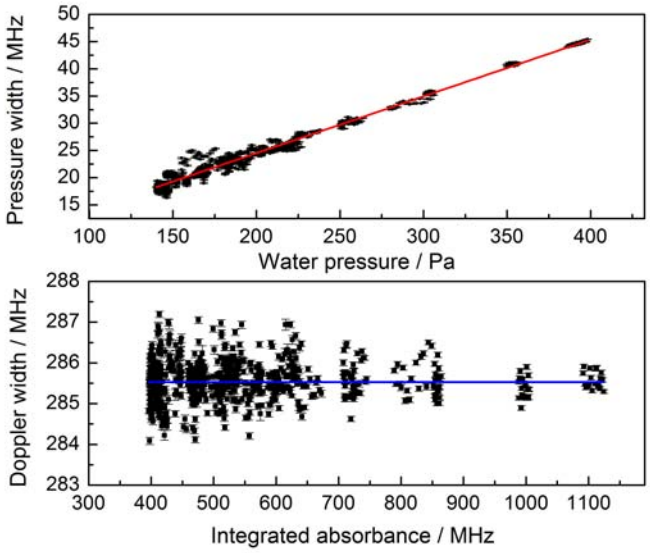

Figure 6. Smoothing of the typical residuals resulting from line fitting to the pcSDHC model. The coherent noise suggests the occurrence of a spurious etalon effect, which is masked by the noise in any spectral acquisition. It must be noted that the largest deviation observed at the low-frequency edge of the scan can be explained in terms of light absorption in coincidence with $H_2{}^{18}O$ line that is used for the absolute stabilization of the reference laser. Its center frequency is roughly 1.7 GHz away from this edge.